Hindawi
Journal of Chemistry
Volume 2023, Article ID 8838634, 17 pages
https://doi.org/10.1155/2023/8838634

Research Article

Design, Synthesis, and Neurotrophic Effect of Arg-Glu-Arg-Met-Ser-(3,5)-Dimethyladamantan-1-Amine *In Vitro* Evaluations as a Potential NMDAR Antagonist

Xiaozhen Wang,[1] **Ze Li**,[2] **Xiaoyi Zhang**,[3] **Meimei Kang**,[1] **Caizhen Lv**,[1] **Xu Zhang**,[1] **Zhiwei Zhao**,[1] **Yanchuan Wu**,[1] **Penghui Song**,[1] **and Rong Wang**[1,4]

[1]*Department of Central Laboratory, Xuanwu Hospital of Capital Medical University, National Clinical Research Center for Geriatric Diseases, Beijing Geriatric Medical Research Center, Beijing, China*
[2]*Department of Pharmacy, Beijing Friendship Hospital, Capital Medical University, Beijing, China*
[3]*School of Pharmaceutical Sciences, Capital Medical University, Beijing, China*
[4]*Center of Alzheimer's Disease, Beijing Institute for Brain Disorders, Beijing, China*

Correspondence should be addressed to Rong Wang; wangrong@xwh.ccmu.edu.cn

Received 22 February 2023; Revised 15 July 2023; Accepted 2 August 2023; Published 21 August 2023

Academic Editor: Maria N. D. S. Cordeiro

Methyl-D-aspartate receptor (NMDAR) is an ionotropic glutamate receptor and plays an important role in neuronal degradation of Alzheimer's disease (AD). According to molecular modeling docking studies, we have designed the compound Arg-Glu-Arg-Met-Ser-(3,5)-dimethyladamantan-1-amine (RERMS-MEM), consisting of an AβPP 5-mer peptide (RERMS) and memantine (MEM). This compound could dock into the active sites of N-methyl-D-aspartate receptor type 2B (NMDAR2B) with a −64.14 kcal/mol CDOCKER interaction energy. The stability of RERMS-MEM was evaluated through a 50 ns molecular dynamics simulation. The results revealed that the docked ligand-receptor complex was stable. Furthermore, surface plasmon resonance (SPR) revealed that the RERMS-MEM binding affinity to the NMDAR2B fragment exhibited over 15-fold enhancement compared to MEM. The SH-SY5Y cell assays showed that RERMS-MEM or RERMS at concentrations of 0.1, 1, 10, or 50 μM could enhance the metabolic rate, and MEM showed no difference compared to the control and indicated cytotoxic effects at 50 μM. RERMS-MEM at concentrations of 0.01, 0.1, 1, 10, or 50 μM increased the number of viable cells and reduced the release of lactate dehydrogenase (LDH). RERMS at concentrations of 10 or 50 μM was similar to RERMS-MEM for increasing viable cells, and MEM showed no difference compared to the control and decreased the number of viable cells at 50 μM. RERMS-MEM or RERMS at concentrations of 10 or 50 μM could antagonize A$\beta_{25\text{-}35}$-induced cytotoxicity, and MEM at 50 μM strengthened the cytotoxicity effects. The results revealed that RERMS-MEM showed a strong NMDAR-blocking activity as a potential NMDAR antagonist, enhancing the neurotrophic effect and cellular growth in SH-SY5Y cells.

1. Introduction

Alzheimer's disease (AD) is one of the most common neurodegenerative diseases and often the leading cause of dementia in the elderly. It is caused by the interaction of multiple genetic and environmental risk factors [1, 2]. Memory loss correlated with neuronal loss in the hippocampus is the main symptom of AD [3, 4], which plays a critical role in AD-induced brain function injury and neurotoxicity. N-methyl-D-aspartate receptors (NMDARs) are ligand-gated cation channels embedded in the cell membrane of neurons and are critically involved in the pathogenesis of AD. Overexcitation of NMDARs leads to excessive influx of Ca^{2+} through receptor-associated ion channels, resulting in neuronal cell injury or death. N-methyl-D-aspartate receptor type 2B (NMDAR2B), a member of NMDARs family, plays a critical role in spatial learning and memory [5]. Thus, the blockade of NMDAR2B is beneficial

for neuroprotection and the prevention of Aβ-induced neuronal disruption [6]. A new homology-based model of the glutamate binding site of the NMDA receptor NMDAR2B subunit was constructed, satisfactorily explaining the structure-activity relationships among a series of agonists, competitive antagonists, and the glutamate site [7].

According to statistics, there are approximately 47 million people worldwide suffering from dementia, of which 80% are diagnosed with AD [8, 9]. However, there is a lack of effective AD drugs available. The latest drug approved by the USFDA, lecanemab, is a humanized immunoglobulin G1 used for treating patients with mild cognitive impairment or mild dementia. However, due to the absence of efficacy and safety data for AD treatment in the early or late stages, it has not been widely used in countries such as China and Japan [10]. Most AD drugs currently available only target the symptoms of cognitive impairment and cannot prevent disease progression, highlighting the urgent need for the development of safe and effective AD drugs to improve this situation [11].

Molecular docking, molecular dynamics simulation, and ADMET prediction are essential methods in computer-aided drug design. Precise design methods for protein-ligand docking are crucial for identifying novel compounds in drug discovery [12]. Molecular docking enables the effective prediction of binding modes and binding affinities in a protein-ligand complex. Molecular dynamics simulation allows for the analysis of conformational changes in the ligand-receptor complex under physiologically relevant conditions, and the identification of key residues is involved in ligand-receptor interactions [13]. ADMET prediction provides insights into drug properties such as absorption, distribution, metabolism, excretion, and toxicity. These powerful tools have been extensively employed in various aspects of drug development research.

The polycyclic amine memantine (MEM), which is a low-affinity voltage-dependent uncompetitive antagonist of NMDARs, is currently used in combination with other acetylcholinesterase inhibitors in the treatment of AD, such as galantamine, donepezil, and rivastigmine [14–17]. Data from preclinical studies suggested that MEM might prevent apoptotic neuronal damage and exert cytoprotective effects [18, 19]. However, high-dose MEM could exert ataxic and amnesic effects in rats and humans [20]. In the search for a disease-modifying drug for AD, MEM could be viewed as a privileged NMDAR-directed structure and represents the driving motif in the design of a variety of multifunctional compounds [21]. Accordingly, a series of studies have focused on the discovery of NMDAR antagonists, such as 7-MEOTA-amantadine hybrids [22, 23], 6-Cl-THA-memantine hybrid [24], memantine-galantamine hybrids [25], carbazole/tetrahydro carbazole-amino adamantane hybrids [26], ferulic acid-memantine hybrid [27], lipoic acid-memantine hybrid [28], propargyl-amantadine hybrids [29], polyamine-memantine hybrids [30], N′-aryl carbohydrazide-amino adamantane hybrid [31], and other research studies [32]. AβPP 17-mer peptide (AβPP 17) is a peptide extracted from the soluble amyloid precursor protein (AβPP), which is neurotrophic with susceptibility to enzymatic degradation [33]. AβPP 5-mer peptide (RERMS) is an active form of AβPP 17 [34] and the analogue of which not only showed neurotrophic effects in SH-SY5Y cells but also resisted pepsin digestion [35]. Moreover, some research studies have demonstrated that RER and its derivatives may enhance the neurotrophic effects in the early stage of Alzheimer's disease [36].

Accordingly, we aimed to design and synthesize a compound with the structure of RERMS and MEM, namely, structure Arg-Glu-Arg-Met-Ser-(3,5)-dimethyladamantan-1-amine (RERMS-MEM) (Figure 1) and evaluate the neurotrophic effect as a potential NMDAR antagonist. In the structure of RERMS-MEM, the original framework of memantine is retained, and modifications on memantine do not affect its blocking effect on NMDA [27]. The modification of RERMS increases the number of binding sites between the compound and NMDAR, enhancing its antagonistic effect on NMDAR.

2. Materials and Methods

2.1. General Information. All syntheses and bioassays were environmentally friendly without potential safety or environmental hazards. Protected amino acids with *L*-configuration were purchased from Sigma Chemical Co. (MO, USA). Chromatography was conducted on Qingdao silica gel H. The purity of RERMS-MEM and its intermediates was analyzed by thin-layer chromatography (TLC) (Qingdao silica gel F254, 0.25-mm layer thickness) or high-performance liquid chromatography (HPLC) (SHIMADZU, JPN), YMC-Pack ODS-A (10×250 mm, 5 μm; YMC). ^{1}H NMR 300 MHz was recorded on a Bruker Avance II-500 spectrometer with DMSO-d_6 as the solvent and tetramethylsilane as an internal standard. ESI/MS was conducted on a mass spectrometer (ZQ 2000; Waters) with a dual ion source of ESI/matrix-assisted laser desorption ionization. Cell count and viability assays were conducted on a Muse® Cell Analyzer. Statistical analyses of biological data were carried out using the *T*-test, and p values <0.05 were considered statistically significant.

SH-SY5Y cells were purchased from American type culture collection (ATCC, USA) within six months. The cells were grown in Dulbecco's modified Eagle's medium (Gibco BRL, New York, USA) containing 10% heat-inactivated foetal bovine serum (Hyclone, Los Angeles, CA, USA), penicillin (100 IU/ml), and streptomycin (100 μg/ml) in T_{75} tissue culture flasks under 95% air, 5% CO_2, and 37°C. 3-(4,5-dimethylthiazol-2-yl)-2,5-diphenyltetrazolium bromide (MTT) assay, cell counting kit-8 (CCK-8), and Aβ_{25-35} and lactate dehydrogenase (LDH) assay kits were purchased from Beyotime. Muse™ Count & Viability Kit was obtained from Merck Millipore. NMDAR2B protein fragment was purchased from Beijing Protein Innovation Co., Ltd.

2.2. Docking of RERMS-MEM toward the Active Site of NMDAR. Software AutoDock 4 was used to perform the docking of 10 energy-optimized conformations of RERMS-MEM toward NMDAR (PDB ID: 5UN1) [6]. NMDAR was treated as rigid and prepared by

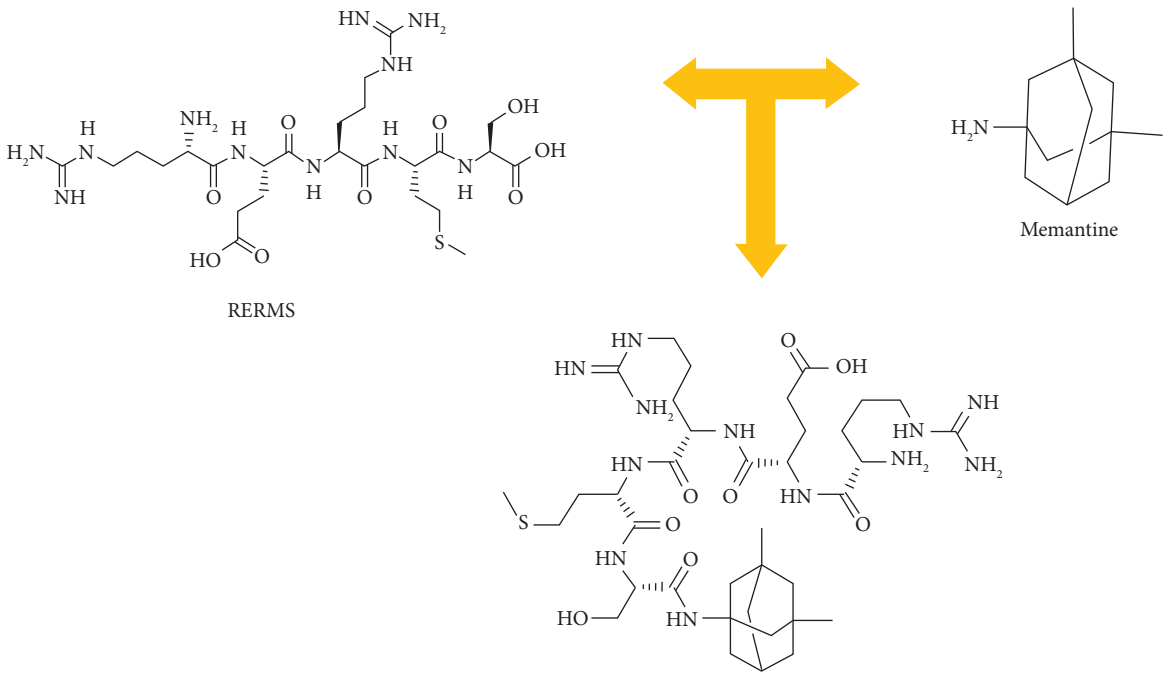

Figure 1: Design and structures of RERMS-MEM.

AutoDockTools 1.5, merging nonpolar hydrogens and assigning Gasteiger charges and AutoDock elements. The 10 energy-optimized conformations of the compounds were treated as rigid ligands and prepared by AutoDockTools 1.5, merging nonpolar hydrogens, assigning Gasteiger charges, finding the root and aromatic carbons, detecting rotatable bonds, and setting torsions. The grid box dimensions were set to 50 Å × 50 Å × 50 Å with a grid spacing of 0.375 Å. The Lamarckian genetic algorithm (LGA) was used to find the appropriate binding positions, orientations, and conformations of the compounds in the active site of NMDAR. The global optimization was started with parameters of a population of 300 randomly positioned individuals. The maximum number of energy evaluations was increased to 2.5×10^7, and the maximum number of generations in the LGA was increased to 2.7×10^5. The Solis and Wets local search was performed with a maximum number of 3000. During docking experiments, 200 runs were carried out for each compound. The resulting 200 conformations of each compound were scored by the lowest binding energy and clustered with an RMS tolerance of 2.0 Å.

2.3. Molecular Dynamics Simulation Studies. The GROMACS 2020.3 software was utilized to conduct molecular dynamics (MD) simulations. For parameter and topology generation of proteins and ligands, the amber99sb-ildn force field and the general amber force field (GAFF) were employed, respectively. The simulation box size was optimized to ensure a minimum distance of 1.0 nm between each atom of the protein and the box. Subsequently, the box was filled with water molecules based on a density of 1. To maintain electrical neutrality, Cl− and Na+ions were introduced to replace the water molecules. To minimize energy consumption and eliminate unreasonable contacts or atom overlap, an energy optimization step consisting of 5.0 × 104 iterations using the steepest descent method was performed on the entire system. Following energy minimization, a preliminary equilibration phase was conducted for 100 ps under the NVT ensemble at 300 K to stabilize the system's temperature. Subsequently, a second equilibration phase was simulated under the NPT ensemble at 1 bar and 100 ps. The primary aim of these simulations was to optimize the interaction among the target protein, solvent, and ions, ensuring a fully pre-equilibrated simulation system. All MD simulations were conducted for 50 ns under an isothermal and isostatic ensemble, maintaining a temperature of 300 K and a pressure of 1 atmosphere. Temperature control was achieved using the V-rescale method, while pressure control employed the Parrinello–Rahman method. The temperature and pressure coupling constants were set to 0.1 and 0.5 ps, respectively. The Van der Waals force was calculated using the Lennard–Jones function, with a nonbond truncation distance of 1.4 nm. The LINCS algorithm was applied to constrain the bond lengths of all atoms. Furthermore, the particle mesh Ewald method with a Fourier spacing of 0.16 nm was utilized to calculate long-range electrostatic interactions.

2.4. ADMET Prediction. Software AutoDock 4 was used to predict the ADMET of RERMS-MEM. Import the small molecule compounds. Open the ADMET Descriptors dialog

box. In the "Input Ligands" section, select all the small molecule compounds. In the "ADMET Descriptors" section, choose the default settings, which select all ADMET properties. Run the calculation workflow to initiate the job. Once the job is completed, click on "View Results" to perform result analysis.

2.5. Peptide Synthesis [37, 38]

2.5.1. Preparing Boc-Arg (NO_2)-Met-OBzl. A solution of 2.5 g (7.85 mmol) of Boc-Arg (NO_2), 1.25 g (9.25 mmol) of hydroxybenzotriazole (HOBt), 1.65 g (9.3 mmol) of N, N′-dicyclohexylcarbodiimide (DCC) in 30 mL of anhydrous tetrahydrofuran (THF) was stirred at 0°C for 30 min. Then, a solution of 3.20 g (7.80 mmol) of Tos Met-OBzl in 10 mL of anhydrous THF was added, and the pH was adjusted to pH 9 with N-methyl morpholine (NMM). The reaction mixture was stirred at room temperature for 12 h, and TLC (CH_2Cl_2/CH_3OH, 30/1) was used to indicate the complete disappearance of Tos Met-OBzl. The resulting dicyclohexylurea was removed by filtration, and the filtrate was evaporated under reduced pressure. The residue was dissolved in 50 mL of ethyl acetate and washed successively with aqueous sodium bicarbonate (5%), aqueous citric acid (5%), and saturated aqueous sodium chloride. The organic layer was separated, dried over anhydrous sodium sulfate, filtered, and evaporated under reduced pressure to yield 3.1 g (74%) of the title compound as a colorless powder.

2.5.2. Preparing Boc-Arg (NO_2)-Met. A solution of 2.5 g (4.6 mmol) of Boc-Arg (NO_2)-Met-OBzl in 30 mL of methanol was stirred at 0°C, to which 10 mL of aqueous NaOH (2 M) was added dropwise. The reaction mixture was stirred for 5 h, and TLC (CH_2Cl_2/CH_3OH, 30/1) was used to indicate the complete disappearance of Boc-Arg (NO_2)-Met-OBzl. After filtration, the filtrate was evaporated under reduced pressure. The residue was dissolved in 30 mL of water and then adjusted to pH 2 with hydrochloric acid (2 M). The formed precipitates were dissolved in 50 mL of ethyl acetate and washed successively with aqueous sodium bicarbonate (5%), aqueous citric acid (5%), and saturated aqueous sodium chloride. The organic layer was separated, dried over anhydrous sodium sulfate, filtered, and then evaporated under reduced pressure to obtain 2.04 g (98%) of the title compound as a colorless powder.

*2.5.3. Preparing N-Boc-Ser-(3,5)-dimethyladamantan-1-amine(**1**).* A solution of 1.95 g (9.5 mmol) of Boc-*L*-Ser, 1.5 g (11.1 mmol) of HOBt, and 4.22 g (11.1 mmol) of 2-(7-azabenzotriazol-1-yl)-N,N,N′,N′-tetramethyluronium hexafluorophosphate (HATU) in 30 mL of anhydrous N, N-dimethylformamide (DMF) was stirred at 0°C for 30 min, to which a solution of 2.16 g (10.0 mmol) of MEM in 10 mL of anhydrous DMF was added and adjusted to pH 9 with NMM. The reaction mixture was stirred at room temperature for 12 h, and TLC (CH_2Cl_2/CH_3OH, 30/1) was used to indicate the complete disappearance of Boc-*L*-Ser. The filtrate was evaporated under reduced pressure. The residue was dissolved in 50 mL of ethyl acetate and washed successively with aqueous sodium bicarbonate (5%), aqueous citric acid (5%), and saturated aqueous sodium chloride. The organic layer was separated, dried over anhydrous sodium sulfate, filtered, and evaporated under reduced pressure to yield 2.7 g (78%) of the title compound as a colorless powder.

2.5.4. Preparing Ser-(3,5)-dimethyladamantan-1-amine. A solution of 2.5 g (6.83 mmol) of N-Boc-*L*-Ser-(3,5)-dimethyladamantan-1-amine and 20 mL solution of hydrogen chloride in ethyl acetate (4 M) was stirred at 0°C for 30 min and subsequently evaporated under vacuum. The residue was dissolved in 10 mL ethyl acetate. The solution was then evaporated under vacuum to thoroughly remove the free hydrogen chloride and obtain 1.96 g (95%) of the title compound as a colorless powder. ESI-MS (M/z): 267.3 $[M+H]^+$.

2.5.5. Preparing N-Boc-Arg (NO_2)-Met-Ser-(3,5)-dimethyladamantan-1-amine. By using the procedure for preparing **1**, from 2.02 g (4.50 mmol) of Boc-Arg (NO_2)-Met and 1.23 g (4.60 mmol) of Ser-(3,5)-dimethyladamantan-1-amine, 1.17 g (36.7%) of the title compound was obtained as a colorless powder. ESI-MS (M/z): 699.6 $[M+H]^+$.

2.5.6. Preparing Arg (NO_2)-Met-Ser-(3,5)-dimethyladamantan-1-amine. A solution of 1.17 g (1.67 mmol) of N-Boc-Arg (NO_2)-Met-Ser-(3,5)-dimethyladamantan-1-amine and 20 mL solution of hydrogen chloride in ethyl acetate (4 M) was stirred at 0°C for 30 min and evaporated under vacuum. The residue was dissolved in 10 mL ethyl acetate. The solution was then evaporated under vacuum to thoroughly remove the free hydrogen chloride and obtain 1.05 g (99%) of the title compound as a colorless powder. ESI-MS (M/z): 599.4 $[M+H]^+$.

2.5.7. Preparing N-Boc-Glu (OBzl)-Arg (NO_2)-Met-Ser-(3,5)-dimethyladamantan-1-amine. By using the procedure for preparing **1**, from 0.67 g (1.98 mmol) of Boc-Glu (OBzl) and 1.05 g (1.66 mmol) of Arg (NO_2)-Met-Ser-(3,5)-dimethyladamantan-1-amine, 0.68 g (45.0%) of the title compound was obtained as a colorless powder. ESI-MS (M/z): 918.8 $[M+H]^+$.

2.5.8. Preparing Glu (OBzl)-Arg (NO_2)-Met-Ser-(3,5)-dimethyladamantan-1-amine. At 0°C, 0.68 g (0.74 mmol) of N-Boc-Glu (OBzl)-Arg (NO_2)-Met-Ser-(3,5)-dimethyladamantan-1-amine was stirred in a solution of hydrogen chloride in 20 mL ethyl acetate (4 M) for 30 min, evaporated under vacuum, and the residue was dissolved in 10 mL ethyl acetate. The solution was evaporated under vacuum to thoroughly remove the free hydrogen chloride and yield 0.63 g (99%) of the title compound as a colorless powder. ESI-MS (M/z): 818.6 $[M+H]^+$.

2.5.9. Preparing N-Boc-Arg (NO_2)-Glu (OBzl)-Arg (NO_2)-Met-Ser-(3,5)-dimethyladamantan-1-amine. By using the procedure for preparing **1**, from 0.26 g (0.80 mmol) of Boc-Arg (NO_2) and 0.60 g (0.70 mmol) of Glu (OBzl)-Arg (NO_2)-Met-Ser-(3,5)-dimethyladamantan-1-amine, 0.20 g (25.1%) of the title compound was obtained as a colorless powder. ESI-Q-TOF-MS (M/z): 1119.0781 $[M+H]^+$. ^1H NMR (DMSO-d_6, 300 MHz) δ/ppm = 8.470 (m, 1H), 8.111 (m, 2H), 7.894 (m, 1H), 7.802 (m, 1H), 7.355 (s, 6H), 7.004 (m, 1H), 5.079 (s, 2H), 4.340 (m, 4H), 4.164 (m, 1H), 3.897 (m, 1H), 3.562 (m, 2H), 3.132 (m, 5H), 2.396 (m, 5H), 2.026 (m, 5H), 1.916 (m, 2H), 1.835 (m, 1H), 1.787 (m, 1H), 1.720 (m, 3H), 1.542 (m, 12H), 1.354 (m, 10H), 1.245 (m, 4H), 1.082 (s, 2H), 0.795 (s, 6H). The ESI (+)-Q-TOF-MS and ^1H NMR of N-Boc-Arg (NO_2)-Glu (OBzl)-Arg (NO_2)-Met-Ser-(3,5)-dimethyladamantan-1-amine were supplied as experiment data (Figure S5-6).

2.5.10. Preparing Arg-Glu-Arg-Met-Ser-(3,5)-dimethyladamantan-1-amine (RERMS-MEM). To a solution of 4 mL of CF_3CO_2H and 1 mL of CF_3SO_3H, 50 mg (0.04 mmol) of N-Boc-Arg (NO_2)-Glu (OBzl)-Arg (NO_2)-Met-Ser-(3,5)-dimethyladamantan-1-amine was added, and the mixture was stirred at 0°C for 1 h. Upon removal of CF_3CO_2H and CF_3SO_3H, the residue was triturated with 100 mL of anhydrous ether and the residue was purified on a pre-HPLC (CH_3CN and 0.1 CF_3COOH/H_2O, 30/70–50/50, 60 min, 220 nm, Kromasil C18, 10 μm, 100 Å, 5 cm, 1 mL/min) to obtain 28 mg (28%) of the title compound as a colorless powder. ESI (+)-FT-ICR-MS (M/z): 839.50042 $[M+H]^+$. ^1H NMR (DMSO-d_6, 800 MHz) δ/ppm = 8.568 (m, 1H), 8.212 (m, 1H), 8.121 (s, 4H), 8.875 (m, 1H), 7.600 (s, 1H), 7.529 (s, 1H), 7.165 (m, 2H), 6.912 (m, 3H), 4.882 (s, 1H), 4.365 (m, 2H), 4.193 (m, 2H), 3.819 (s, 1H), 3.524 (m, 2H), 3.105 (s, 4H), 2.437 (m, 3H), 2.290 (m, 2H), 2.097 (m, 4H), 1.924 (m, 2H), 1.727 (m, 7H), 1.533 (m, 9H), 1.269 (dd, J_1 = 12 Hz, J_2 = 40 Hz, 5H), 1.092 (m, 2H), 0.803 (s, 6H). ^{13}C NMR (DMSO-d_6, 200 MHz) δ/ppm = 173.33, 170.59, 170.15, 169.99, 168.28, 167.65, 157.70, 157.54, 157.39, 157.24, 156.10, 156.07, 118.85, 117.35, 115.86, 114.37, 61.08, 54.79, 51.85, 51.26, 51.23, 51.17, 49.58, 46.37, 41.64, 39.96, 39.56, 31.68, 31.24, 29.45, 28.86, 28.80, 28.21, 27.73, 27.23, 24.40, 23.53, 14.08. HPLC purity (CH_3CN and 0.1 CF_3COOH/H_2O, 25/75–45/55, 20 min, 220 nm, Unitary C18, 5 μm, 100 Å 4.6 ∗ 150 mm, 1 mL/min): 98%. The ESI (+)-FT-ICR-MS, ^1H NMR, ^{13}C NMR, HPLC of RERMS-MEM were supplied as experiment data (Figure S1-4).

2.6. Surface Plasmon Resonance (SPR) Assay. Following the abovementioned molecular docking results, the NMDAR2B protein fragment was selected for SPR analysis of RERMS-MEM, RERMS, and MEM. The sequence of the protein fragment was FEYFSPVGYNRCLADGREPGGPSFTIGKA IWLLWGLVFNNSVPVQNPKGTTSKIGSTANLAAFMIQE EYVDQVSGLSDKKFQRPNDFSPPFRFGTVPNGSTERNIR NNYAEMHAYMGKFNQRGVDDALLSLKTGKLDAFIYDA AVLNYMAGRDEGCKLVTIGSGKVFASTGYGIAIQKDSGW KRQVDLAILQLFGDGEMEELEALWLTGICHNEKNEVM SSQLDIDN (containing the active sites of NMDAR). SPR assays were performed by using a Biacore 8 k system (Cytiva) with three steps. The first step was protein immobilization. Proteins were diluted in sodium acetate solution (GE Healthcare) and immobilized on a CM5 chip through a 1-ethyl-3-(3-dimethylaminopropyl) carbodiimide hydrochloride/N-hydroxy sulfo succinimide (EDC/NHS) reaction. Subsequently, affinity detection was performed according to the operating protocol provided by GE Healthcare. Diluted RERMS-MEM, RERMS, and MEM were added to concentrations of 6.25–200 μM in the running buffer. The analytes were injected into the system at a flow rate of 30 μL/min, while the association and dissociation times were 120 s and 400 s, respectively. The association and dissociation processes were all conducted in the running buffer. In the last step of data processing, the affinity curve fitting was carried out with Biacore insight evaluation software. A steady-state affinity model was used for the curve fitting, and the dissociation equilibrium constant (K_D) was also calculated. The Rmax was calculated according to the immobilization level. The SPR assay adopts a double deduction system, and the negative signal is automatically deducted by the instrument.

2.7. MTT Assay. SH-SY5Y cells were seeded onto 96-well plates (~3×10^4 cell/well) and grown until reaching 80% confluence. Cells were either untreated (control) or treated with MEM, RERMS, or RERMS-MEM at concentrations of 0.01, 0.1, 1, 10, or 50 μM for 48 h. The cells were then exposed to MTT (5 mg/mL) to measure the metabolic rate. The MTT assay was performed by incubating the cells with MTT solution for 4 h at 37°C. The formed formazan was dissolved in dimethyl sulfoxide (DMSO). Cell viability was calculated by measuring the absorbance at 570 nm. Statistical analysis was performed using the SPSS 19.0 program, and a significance level of $p < 0.05$ was considered to indicate statistical significance.

2.8. CCK-8 Assay. The CCK-8 assay was performed according to instructions of the CCK-8 assay kit used. SH-SY5Y cells were seeded onto 96-well plates (~3×10^4 cell/well) and grown until reaching 80% confluence. Cells were untreated (control) or exposed to MEM, RERMS, or RERMS-MEM at 0.01, 0.1, 1, 10, or 50 μM for 48 h. Next, 10 μL of CCK-8 solution was added to each well, and the cells were incubated at 37°C for 4 h. Cell viability was calculated by measuring the absorbance at 450 nm. Statistical analysis was performed with SPSS 19.0, with $p < 0.05$ considered to indicate significance.

2.9. Cell Count and Viability Assay. SH-SY5Y cells were seeded onto 24-well plates (~3×10^4 cell/well) and allowed to grow for 4 h. Next, the cells were untreated (control) or exposed to MEM or RERMS at 10 or 50 μM or to RERMS-MEM at 0.01, 0.1, 1, 10, or 50 μM for 48 or 96 h. The cells were made into a single-cell suspension. Next, 50 μL of cell solution was added to 450 μL of Muse Count & Viability Kit reagent and incubated at room temperature for 5 min. The incubated samples were put into Muse® Cell Analyzer for testing, and the number of total cells including live cells

and dead cells were measured. Statistical analysis was performed by using SPSS 19.0, and differences with $p < 0.01$ were considered significant.

2.10. LDH Release Assay. SH-SY5Y cells were seeded onto 96-well plates ($\sim 3 \times 10^4$ cell/well) and allowed to grow to 80% confluence. Cells were untreated (control) or exposed to RERMS at 0.01, 0.1, or 1 μM for 24 h. The supernatant from each well was collected. The LDH activity assay kit was used to measure the LDH activity according to the manufacturer's instructions. Statistical analysis was performed by using SPSS 19.0, and $p < 0.01$ was considered significant.

2.11. RERMS-MEM Antagonized the A$\beta_{25\text{-}35}$-Induced Cytotoxicity. SH-SY5Y cells were seeded onto 96-well plates ($\sim 3 \times 10^4$ cell/well) and grown until reaching 80% confluence. Cells were treated with Aβ_{25-35} of 0.1, 1, 10, 20, or 50 μM as a toxicity screening group, treated with Aβ_{25-35} of 20 μM and compounds (including MEM, RERMS, and RERMS-MEM) of 0.1, 1, 10, or 50 μM as drug intervention groups, and untreated as the control group for 24 h, respectively. All the groups of cells were then exposed to MTT (5 mg/mL) to measure the metabolic rate. The MTT assay was performed by incubating the cells with MTT solution for 4 h at 37°C. The formed formazan was dissolved in DMSO. Cell viability was calculated by measuring the absorbance at 570 nm. Statistical analysis was performed using the SPSS 19.0 program.

3. Results

3.1. Docking of RERMS-MEM toward the Active Site of NMDAR. The molecular docking software AutoDock 4 was used to simulate the binding mode of the designed compound and NMDAR (PDB code: 5UN1). Docking of RERMS-MEM into the active sites of NMDAR was −64.14 kcal/mol of CDOCKER interaction energy. The docking interaction energy was lower than the standard ligand of NMDAR with −27.52 kcal/mol (Figure 2). Some interactions were observed between RERMS-MEM and NMDAR (Table 1).

3.2. Molecular Dynamics Simulation Studies. To further investigate the dynamic interactions between the compound and NMDAR and assess the stability of the docked ligand-receptor complex, we conducted molecular dynamics simulations of 50 ns. The RMSD fluctuated during 1–12 ns of simulation and system reached a converged state for the rest of the course with the root mean square deviation (RMSD) values fluctuated between 0.55 and 0.72 nm (Figure 3(a)). The motion changes of individual amino acid residues during molecular dynamics simulations can be captured by the root mean square fluctuation (RMSF). The highest observed flexibilities are related to terminal residues of the protein. The residues 567 (D subunit), 581 (A subunit), 581 (C subunit), 582 (B subunit), 609 (B subunit), 609 (D subunit), 611 (A subunit), and 617 (C subunit) with higher fluctuations belonged to the loop regions. The key active site amino acid residues exhibited rigid behavior in all the system indicating the stability of the compounds in the ligand-receptor complex (Figure 3(b)). The radius of gyration (Rg) is a criterion of system compactness. The smaller Rg indicates a denser protein structure, while a larger value suggests a looser structure. When the Rg value remains stable, the protein is considered stable throughout the entire simulation process. In the simulations of RERMS-MEM and NMDAR, the Rg value gradually decreased and stabilized after 30 ns, indicating that the system could bind stably (Figure 3(c)). Hydrogen bonding is an important non-covalent force that stabilizes protein structures and serves as a measure of stability for ligand-receptor complex. To assess the stability of the complex, we simulated the number of hydrogen bonds formed between the ligand and protein within a duration of 50 ns (Figure 3(d)).

3.3. ADMET Prediction. The ADMET parameters were calculated to investigate the drug-like activity of RERMS-MEM. As shown in Table 1, the predicted levels of solubility were 2, indicating its low water solubility. The BBB-level was 4, indicating a less reliable prediction. The p value prediction of plasma protein binding, cytochrome P450 2D6 inhibition, and hepatotoxicity parameters was small, indicating a less reliable prediction (Table 2).

3.4. Synthesis of RERMS-MEM. An environmentally friendly synthetic route was designed to obtain RERMS-MEM at sufficient levels of purity and yield (Figure 4). Boc-Ser-MEM and Boc-Arg (NO_2)-Met-OBzl were synthesized using conventional condensation agents. Boc-Arg (NO_2)-Met-Ser-MEM was formed (36.7% yield) by coupling Boc-Arg (NO_2)-Met and Ser-MEM after the removal of OBzl and Boc. Boc-Arg (NO_2)-Glu (OBzl)-Arg (NO_2)-Met-Ser-MEM was prepared (11.3% total yield) using the solution method and stepwise synthesis (from the C-terminus to the N-terminus) with Boc-Arg (NO_2), Boc-Glu (OBzl), and Arg (NO_2)-Met-Ser-MEM as materials. Upon removal of all protective groups of Boc-Arg (NO_2)-Glu (OBzl)-Arg (NO_2)-Met-Ser-MEM, RERMS-MEM was obtained at 28% yield. These data suggested that the reaction conditions were mild and the yield of the individual reaction was acceptable.

3.5. SPR Assay. Following the above molecular docking results, SPR was used to measure the binding affinity between NMDAR2B fragment and RERMS-MEM, RERMS, and MEM. The result showed a concentration-dependent increase in resonance signals and demonstrated that all three compounds can strongly bind to the NMDAR2B fragment. Biacore insight evaluation software was used to further confirm the K_D: RERMS-MEM showed the highest response and best affinity to NMDAR2B fragment, in which the K_D values of RERMS-MEM, RERMS, and MEM were 0.601 μM, 2.14 μM, and 9.00 μM, respectively. The K_D value of RERMS-MEM showed a 14.97-fold decrease compared with MEM, which indicated that there is a more powerful affinity between RERMS-MEM and NMDAR2B fragment (Figures 5(a)–5(d)).

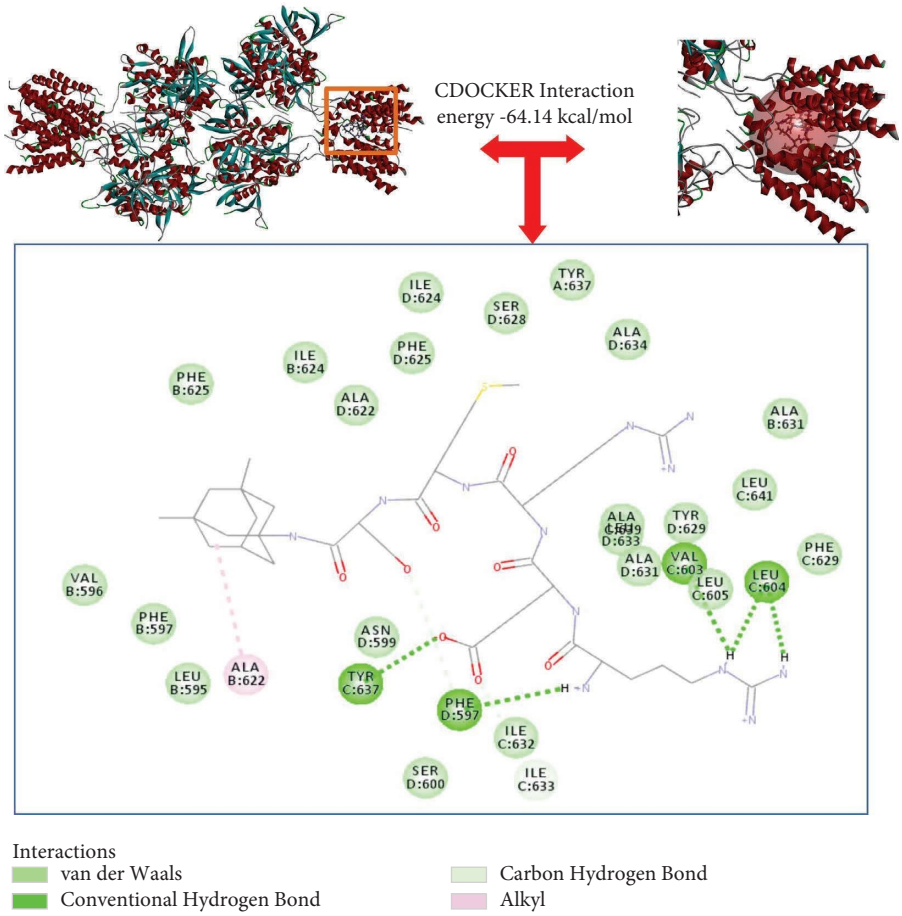

Figure 2: Molecular docking of compound RERMS-MEM with NMDAR.

Table 1: Molecular docking interactions of novel ligands with protein 5UN1.

	Interacting amino acids
Van der Waals	Leu595 (B subunit), Val596 (B subunit), Phe597 (B subunit), Asn599 (D subunit), Ser600 (D subunit), Leu605 (C subunit), Ala622 (D subunit), Ile624 (B subunit), Ile624 (D subunit), Phe625 (B subunit), Phe625 (D subunit), Ser628 (D subunit), Phe629 (C subunit), Tyr629 (D subunit), Ala631 (B subunit), Ala631 (D subunit), Ile632 (C subunit), Ile633 (C subunit), Leu633 (D subunit), Ala634 (D subunit), Tyr637 (A subunit), Ala639 (C subunit), and Leu641 (C subunit)
Conventional hydrogen bond	Phe597 (D subunit), Val603 (C subunit), Leu604 (C subunit), and Tyr637 (C subunit)
Carbon-hydrogen bond	Ile633 (C subunit)
Alkyl	Ala622 (B subunit)

3.6. RERMS-MEM Enhanced the Metabolic Rate. The MTT and CCK-8 test were used to evaluate the metabolic rate effect of RERMS-MEM in SH-SY5Y cells. SH-SY5Y cells were treated with MEM, RERMS, or RERMS-MEM at concentrations of 0.01, 0.1, 1, 10, or 50 μM for 48 h. Results of MTT analysis showed that 0.1, 1, 10, or 50 μM RERMS-MEM or RERMS significantly enhanced the metabolic rate of SH-SY5Y cells compared with the control. Treatment with 0.01 μM of RERMS-MEM or RERMS and 0.01, 0.1, 1 or 10 μM MEM showed no significant difference in the metabolic rate compared with the control. Furthermore, SH-SY5Y cells grew significantly slower after treatment with 50 μM MEM than the control (Figure 6(a)). CCK-8 assays showed similar results as the MTT assay (Figure 6(b)).

3.7. RERMS-MEM Increased the Number of Viable Cells. The cell viability test was used to further explore the neurotrophic effect of RERMS-MEM in SH-SY5Y cells. The results showed that no significant difference was observed in the treatment of 10 μM MEM for 48 or 96 h compared with the control (Figure 7(c)), but a significantly decreased number of viable cells were found at 50 μM MEM compared with the control (Figure 7(d)). Furthermore, a significantly

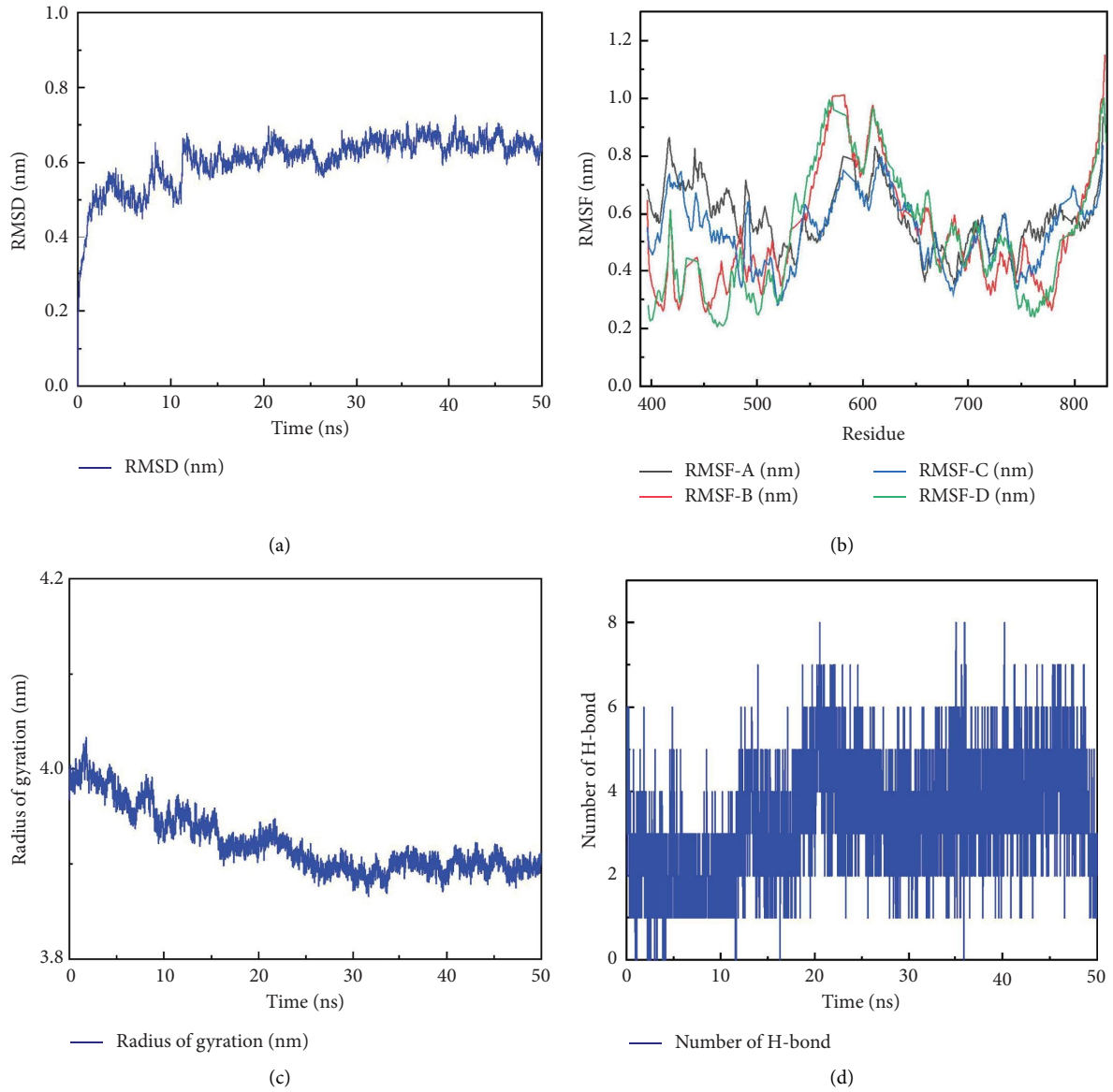

Figure 3: Molecular dynamics simulation studies of compound RERMS-MEM with NMDAR. (a) The RMSD plot of NMDAR with RERMS-MEM. (b) The RMSF plot of each amino acid residues of RERMS-MEM-NMDAR complex during 50 ns. (c) Plot of radius of gyration of backbone atoms of NMDAR in complex with RERMS-MEM. (d) The number of hydrogen bond interactions formed between ligands RERMS-MEM and NMDAR throughout the 50 ns.

increased number of viable cells were observed in the treatment of 10 or 50 μM RERMS-MEM or RERMS for 48 or 96 h compared with the control (Figures 7(c) and 7(d)). The results suggested that 50 μM MEM exerted a cytotoxic effect, whereas 10 μM or 50 μM RERMS-MEM or RERMS showed an increased neurotrophic effect compared with the control.

The abovementioned experiments confirmed that the modification of RERMS can reverse the cytotoxic effect of MEM at 50 μM to SH-SY5Y cells. The neurotrophic effect of lower dose RERMS-MEM was evaluated subsequently, and the result showed that treatment with 0.01, 0.1, and 1 μM RERMS-MEM for 48 or 96 h could increase the number of viable cells compared with the control (Figure 8).

3.8. RERMS-MEM Decreased the Release of LDH. The amount of released LDH is an indicator of cell death; therefore, the LDH assay was used to evaluate the neurotrophic effect of RERMS-MEM in SH-SY5Y cells. Treatment with 0.01, 0.1, 1, 10, or 50 μM RERMS-MEM significantly decreased LDH release compared with the control (Figure 9). Furthermore, a significantly greater decrease in LDH release

Table 2: The ADMET prediction of RERMS-MEM.

Aqueous solubility		BBB penetration		Plasma protein binding	
Solubility	Solubility-level	BBB-level	EXT_PPB	EXT_PPB#MD	EXT_PPB#MD *p*value
−5.541	2 (yes, low)	4 (undefined)	−26.7059	19.9516	$4.72E-23$
Cytochrome P450 2D6 inhibition				Hepatotoxicity	
EXT-CYP2D6	EXT_CYP2D6#MD	EXT_CYP2D6#MD *p*value	EXT_Hepatotoxic	EXT_Hepatotoxic#MD	EXT_Hepatotoxic#MD *p*value
−10.037	34.5636	$1.23E-26$	−18.6621	16.2166	$1.29E-14$

BBB: blood brain barrier.

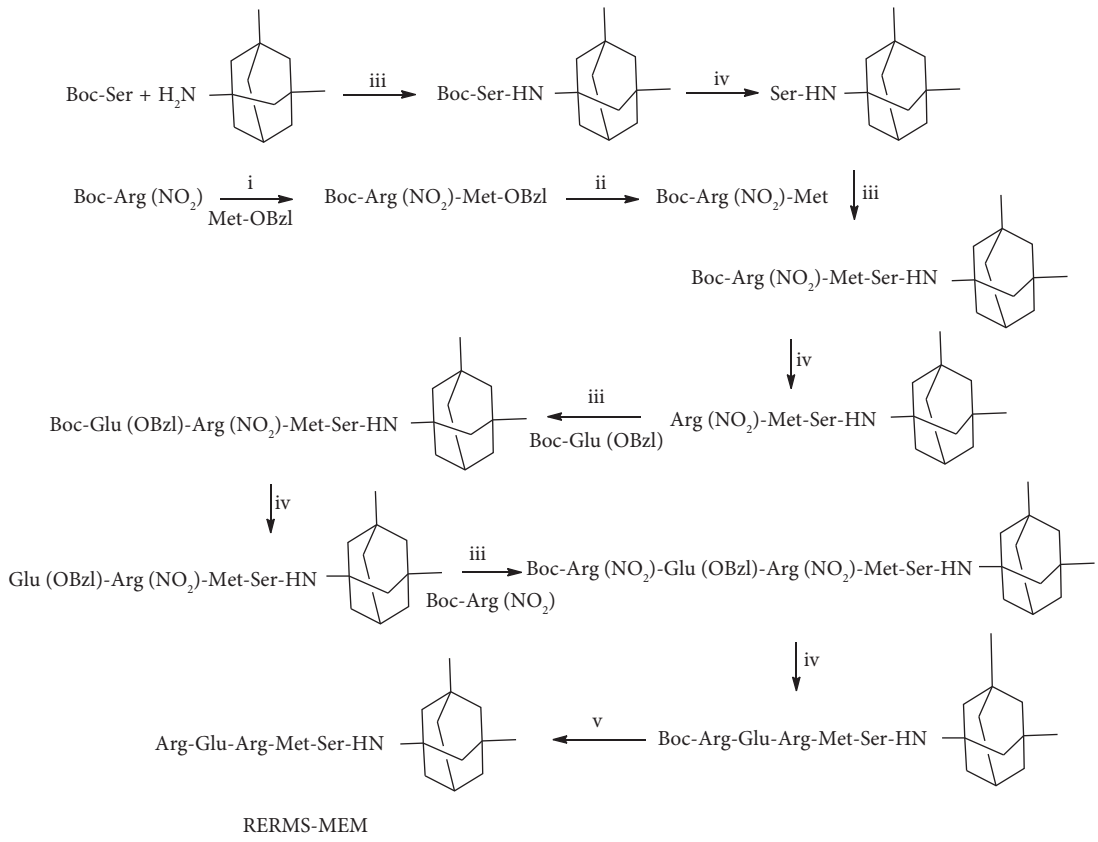

Figure 4: Synthetic route of RERMS-MEM. (i) DCC, HOBt, NMM, and THF; (ii) aqueous NaOH (2 M); (iii) HATU, HOBt, NMM, and DMF; (iv) hydrogen chloride in ethyl acetate (4 M); (v) CF_3CO_2H/CF_3SO_3H. DCC: dicyclohexylcarbodiimide; HOBt: hydroxybenzotriazole; NMM: N-methylmorpholine; THF: tetrahydrofuran; HATU: 2-(7-azabenzotriazol-1-yl)-N,N,N′,N′-tetramethyluronium hexafluorophosphate; DMF: N, N-dimethylformamide.

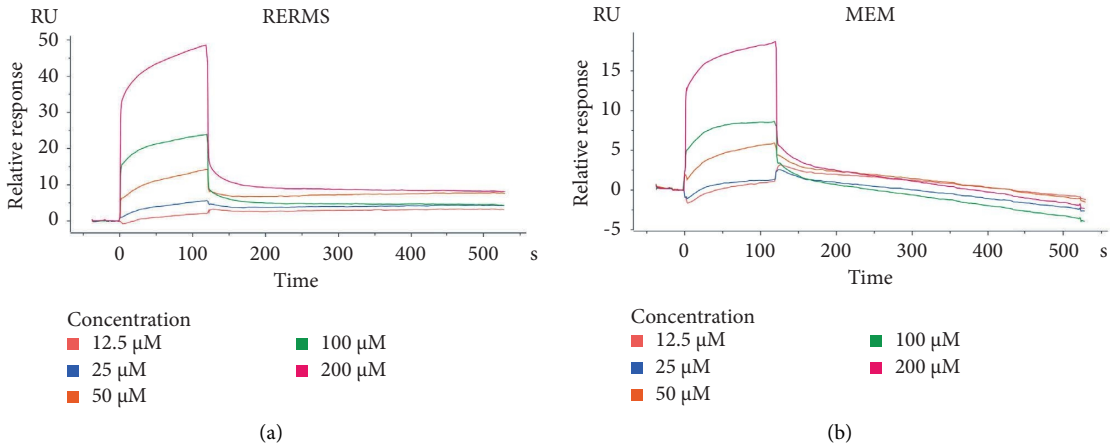

Figure 5: Continued.

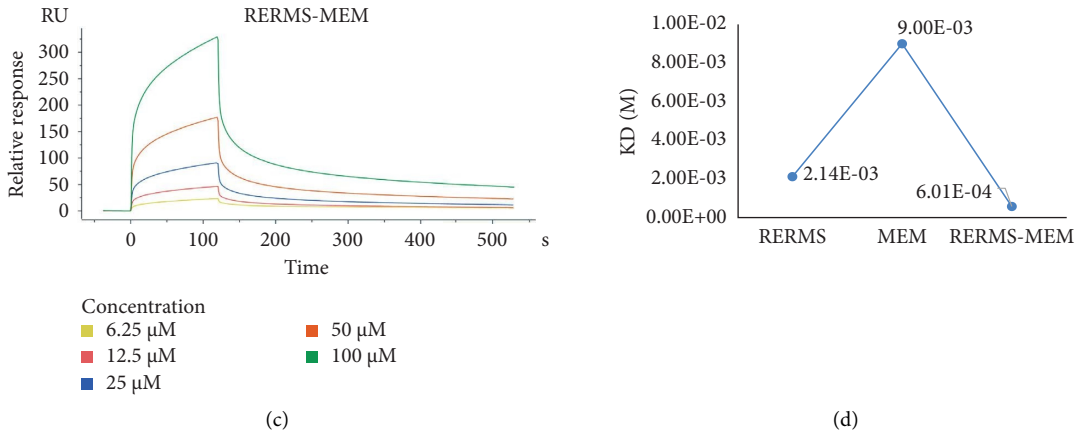

Figure 5: The SPR binding affinity between different concentrations of compounds: (a) RERMS, (b) MEM, (c) RERMS-MEM, and (d) kinetic data from the SPR binding affinity analysis. K_D, dissociation equilibrium constant.

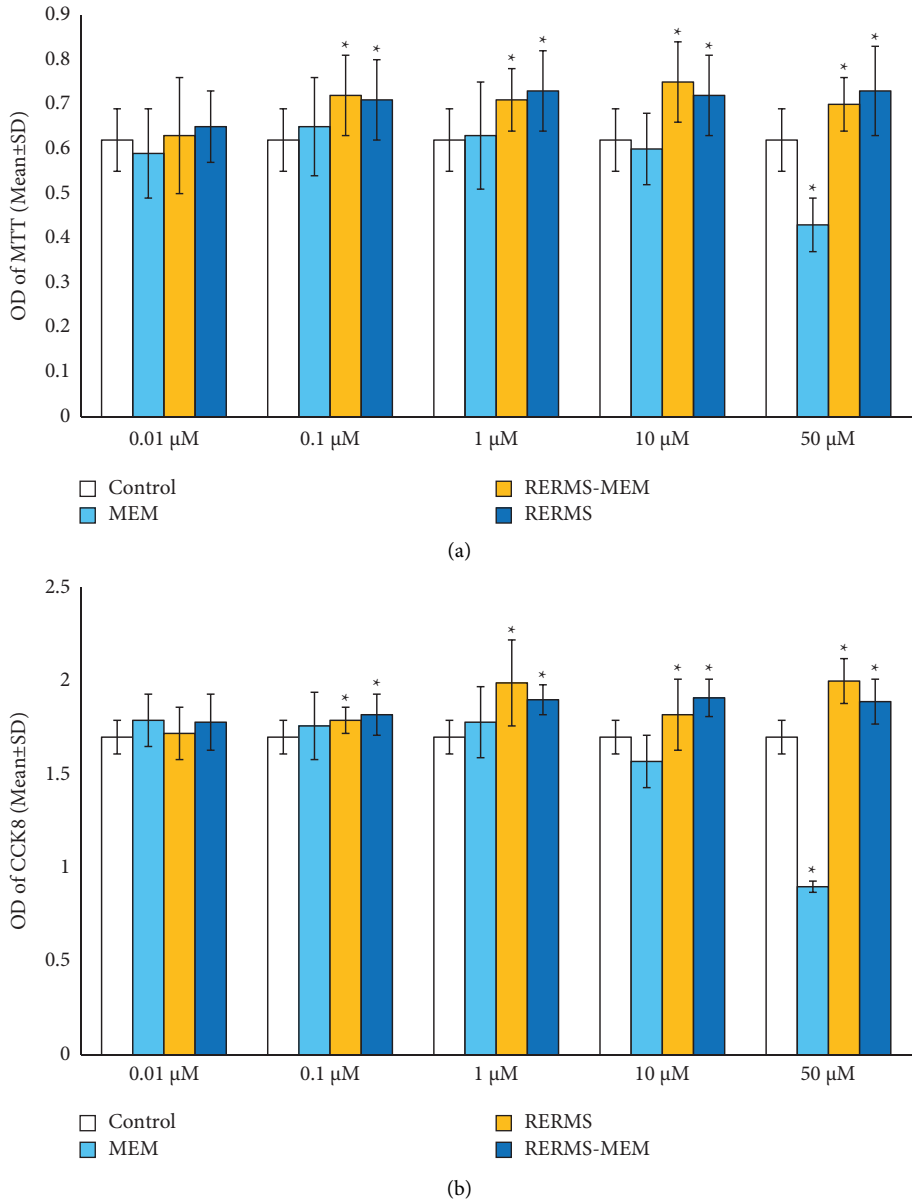

Figure 6: Effect of MEM, RERMS, and RERMS-MEM on the SH-SY5Y cell metabolic rate ($n = 8$). (a) Cell metabolic rate determined by the MTT assay. (b) Cell metabolic rate determined by the CCK-8 assay. $^*p < 0.05$ versus the control. The values are shown as the mean ± SD.

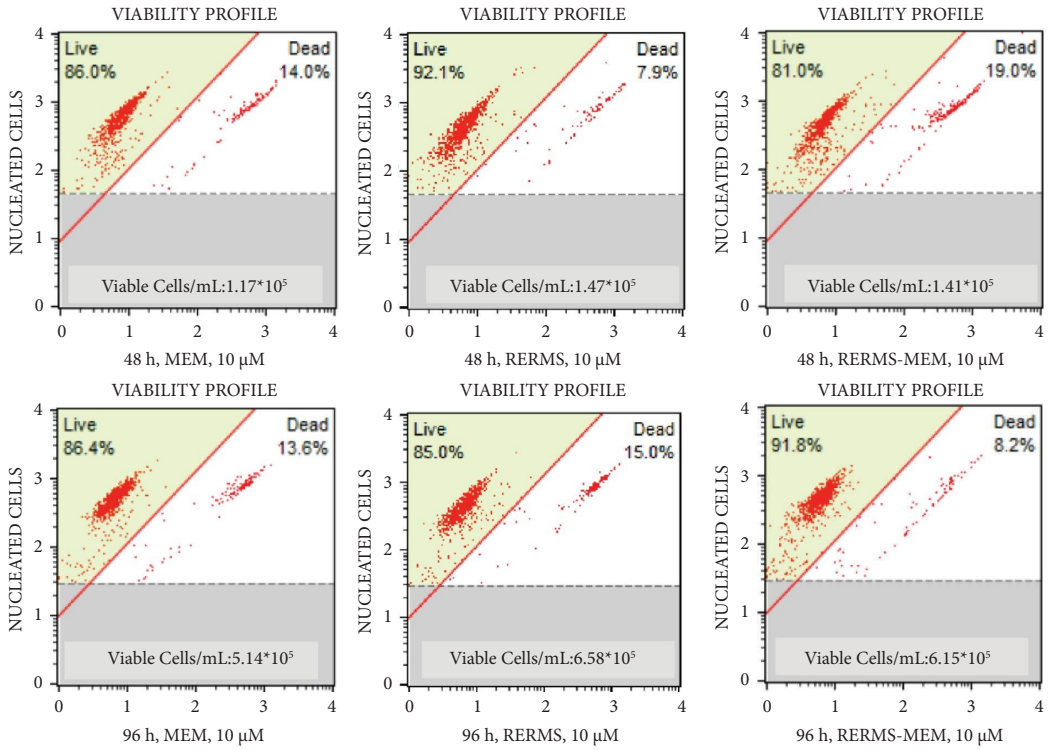

(a)

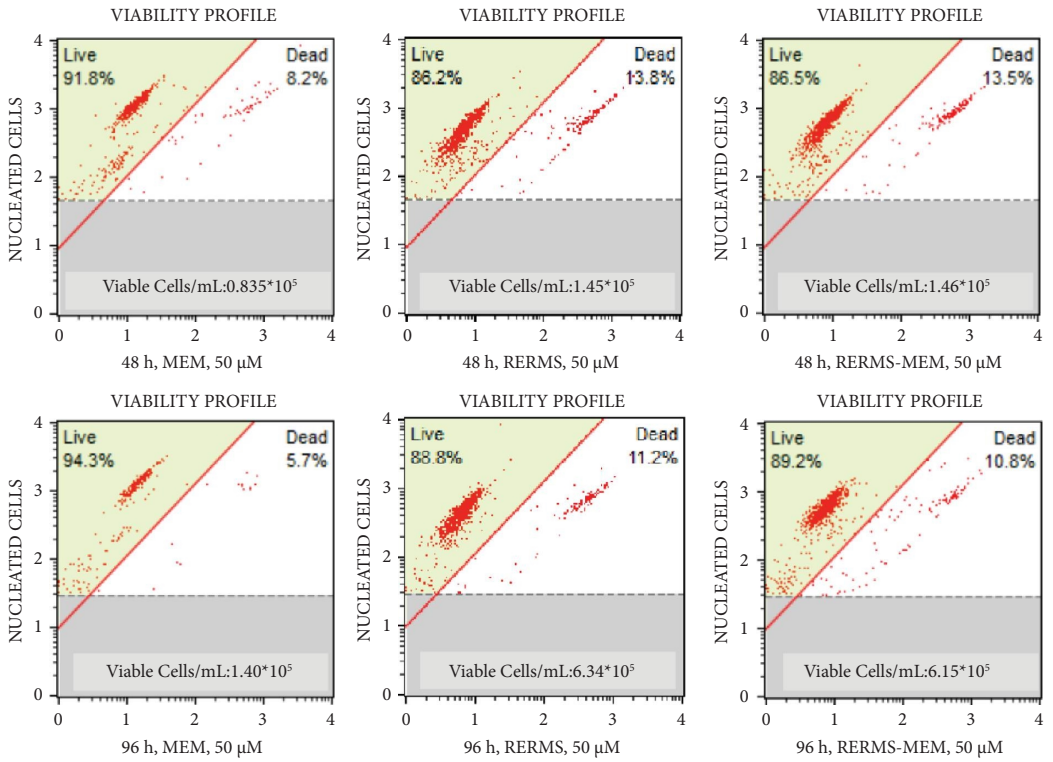

(b)

Figure 7: Continued.

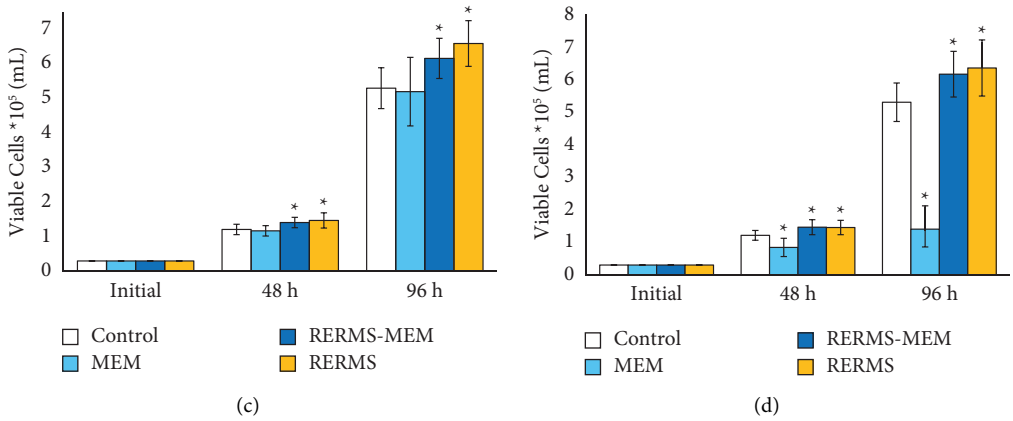

Figure 7: Effect of MEM, RERMS, and RERMS-MEM on the viability of SH-SY5Y cells ($n = 5$). (a) The viability profile graph of treatment with 10 μM MEM, RERMS, or RERMS-MEM. (b) The viability profile graph of treatment with 50 μM MEM, RERMS, or RERMS-MEM. (c) The number of viable cells in treatment with 10 μM MEM, RERMS, or RERMS-MEM. (d) The number of viable cells in treatment with 50 μM MEM, RERMS, or RERMS-MEM. $^*p < 0.05$ versus the control. The values are shown as the mean ± SD.

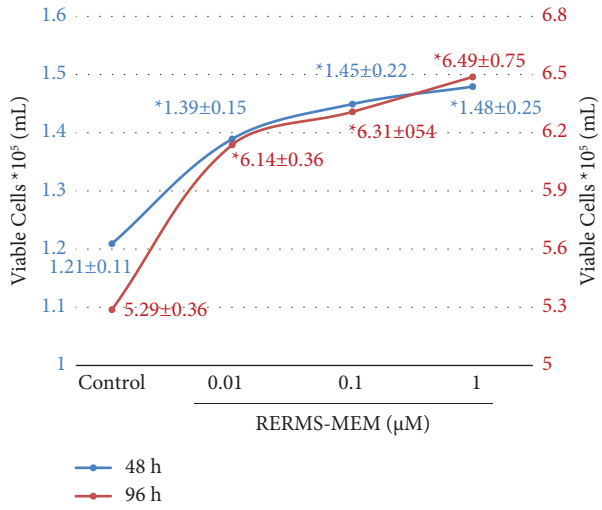

Figure 8: Effect of RERMS-MEM at 0.01, 0.1, or 1 μM on the viability of SH-SY5Y cells ($n = 5$). $^*p < 0.05$ versus the control. The values are shown as the mean ± SD.

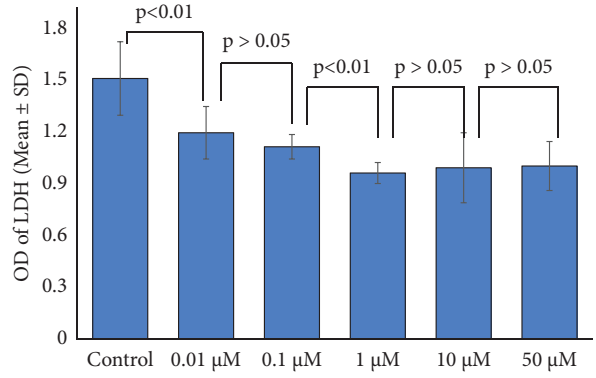

Figure 9: Effect of RERMS-MEM for 24 h on the release of lactate dehydrogenase in SH-SY5Y cells ($n = 8$). The values are shown as the mean ± SD.

was observed in the treatment of 1, 10, or 50 μM RERMS-MEM compared with RERMS-MEM of 0.01, 0.1 μM, suggesting that RERMS-MEM has a neurotrophic effect in SH-SY5Y cells in a concentration-dependent manner as well.

3.9. RERMS-MEM Antagonized the A$\beta_{25\text{-}35}$-Induced Cytotoxicity. Aβ_{25-35} is a widely used neurotoxicity inducer in the study of the cerebral system [39–41]; thus, it was used to investigate the neurotrophic effect of RERMS-MEM in SH-SY5Y cells. Treatment with 0.1, 1, 10, 20, or 50 μM Aβ_{25-35} could induce a cytotoxicity effect on SH-SY5Y cells with a concentration-dependent increase (Figure 10(a)). Treatment with 10 or 50 μM RERMS-MEM or RERMS significantly decreased the A$\beta_{25\text{-}35}$-induced cytotoxicity (Figures 10(b) and 10(d)). Furthermore, treatment with 10 μM MEM significantly decreased the Aβ_{25-35}-induced cytotoxicity; however, treatment with 50 μM MEM increased the Aβ_{25-35}-induced cytotoxicity (Figure 10(c)). The results further confirmed that the antagonistic rate of RERMS-MEM or RERMS for Aβ_{25-35}-induced neurotoxicity on SH-SY5Y cells was more pronounced than MEM, especially at 50 μM (Figure 10(e)).

4. Discussion

AD is a degenerative disease of the central nervous system, in which the loss of neurons is one of the main pathological features. Overexcitation of NMDARs led to neuronal cell injury or death, resulting in neuronal cell loss. MEM, a low-affinity voltage-dependent uncompetitive antagonist of NMDAR, is currently used in combination with other acetylcholinesterase inhibitors in the treatment of AD [14–17]. Mounting evidence has shown that MEM had no clear positive effects in clinical applications although it showed promising results in the preclinical stages [42]. Previous studies revealed that AβPP 5 and AβPP 5 analogues exert a neurotrophic effect in vitro; thus, MEM was modified by AβPP 5 aiming to design a safer and neurotrophic antidementia drug that could enhance the binding affinity with NMDAR.

NMDARs have a domain-layered architecture, with the amino-terminal domain and the ligand- or agonist-binding domain residing in the synaptic space and the transmembrane domain spanning the membrane [43, 44]. The docking investigation indicated that RERMS-MEM could dock into the LBD of NMDAR with lower CDOCKER interaction energy compared with the standard ligand, and twenty-nine interactions including van der Waals, conventional hydrogen bond, carbon-hydrogen bond, and alkyl were observed between RERMS-MEM and NMDAR. Subsequently, a 50 ns molecular dynamics simulation was carried out on the docked complex. The system reached a converged state during 12–50 ns with RMSD values fluctuated between 0.55 and 0.72 nm. The RMSF result reflected the stability of the compound in the ligand-receptor complex. The Rg value gradually decreases and stabilizes after 30 ns, indicating that the system can bind stably. The number of hydrogen bonds formed by NMDAR and RERMS-MEM was found to be from 1 to 8. The results of molecular dynamics simulation studies revealed that the ligand-receptor complex was stable. The ADMET parameters suggested its low water solubility. The BBB-level, plasma protein binding, cytochrome P450 2D6 inhibition, and hepatotoxicity parameters were less reliable predictions. To further definite RERMS-MEM as a potential NMDAR antagonist, the SPR assay was used to display the binding affinity among RERMS-MEM, RERMS, MEM, and NMDAR2B fragment. As a result, RERMS-MEM showed the highest response and most powerful affinity to NMDAR2B fragment. What is more, the K_D value of RERMS-MEM decreased 14.97-fold compared to MEM. The results indicated that there is a strong affinity between RERMS-MEM and NMDAR2B fragment, and it should be attributed to the RERMS modification, which improved the docking feature and led to more amino acid residues of the active site involved in the interactions between RERMS-MEM and NMDAR2B fragment.

We designed a series of cell assays to evaluate the neurotrophic effect of RERMS-MEM. MTT and CCK-8 assays revealed that RERMS-MEM or RERMS of 0.1, 1, 10, or 50 μM could enhance the metabolic rate, but MEM showed no difference compared with the control and indicated a cytotoxicity effect at 50 μM especially. In addition, the result of RERMS-MEM was similar to AβPP 5 analogues [35], which indicated that MEM modified by AβPP 5 exerted a neurotrophic effect on cells. With respect to the cell viability and LDH release assay, RERMS-MEM of 0.01, 0.1, 1, 10, or 50 μM increased the number of viable cells and reduced the release of LDH, RERMS of 10 or 50 μM was similar to RERMS-MEM for increasing viable cells, but MEM showed no difference compared with the control and decreased the number of viable cells at 50 μM. In our opinion, the abovementioned two assays indicated that the mechanism of the neurotrophic effect of RERMS-MEM could be described as metabolic rate enhancement and cellular growth-promoting. Furthermore, RERMS-MEM or RERMS of 10 or 50 μM could more strongly antagonize the Aβ_{25-35}-induced cytotoxicity, but MEM of 50 μM strengthened the cytotoxicity effect. The abovementioned result revealed that RERMS-MEM could improve the safety of MEM (maximum clinical dosage is about 93 μmol/d) by the neurotrophic effect. As we know, adherence to medicine is an assignable problem in the history of drug treatment, especially for the elderly with AD, who are suffering from memory loss and cognition hypofunction [45]. As a result, they might have the risk of overdose and aggravation of adverse reactions. Compared with MEM, the modified compound RERMS-MEM showed no cytotoxicity effect in the same high dose, indicating that it might be safer than MEM. All the cell assays proved that the modification design of RERMS-MEM was successful, which enhanced the neurotrophic effect by promoting the metabolic rate and cellular growth in SH-SY5Y cells. Future work will include cellular experiments investigating the binding between RERMS-MEM and NMDAR.

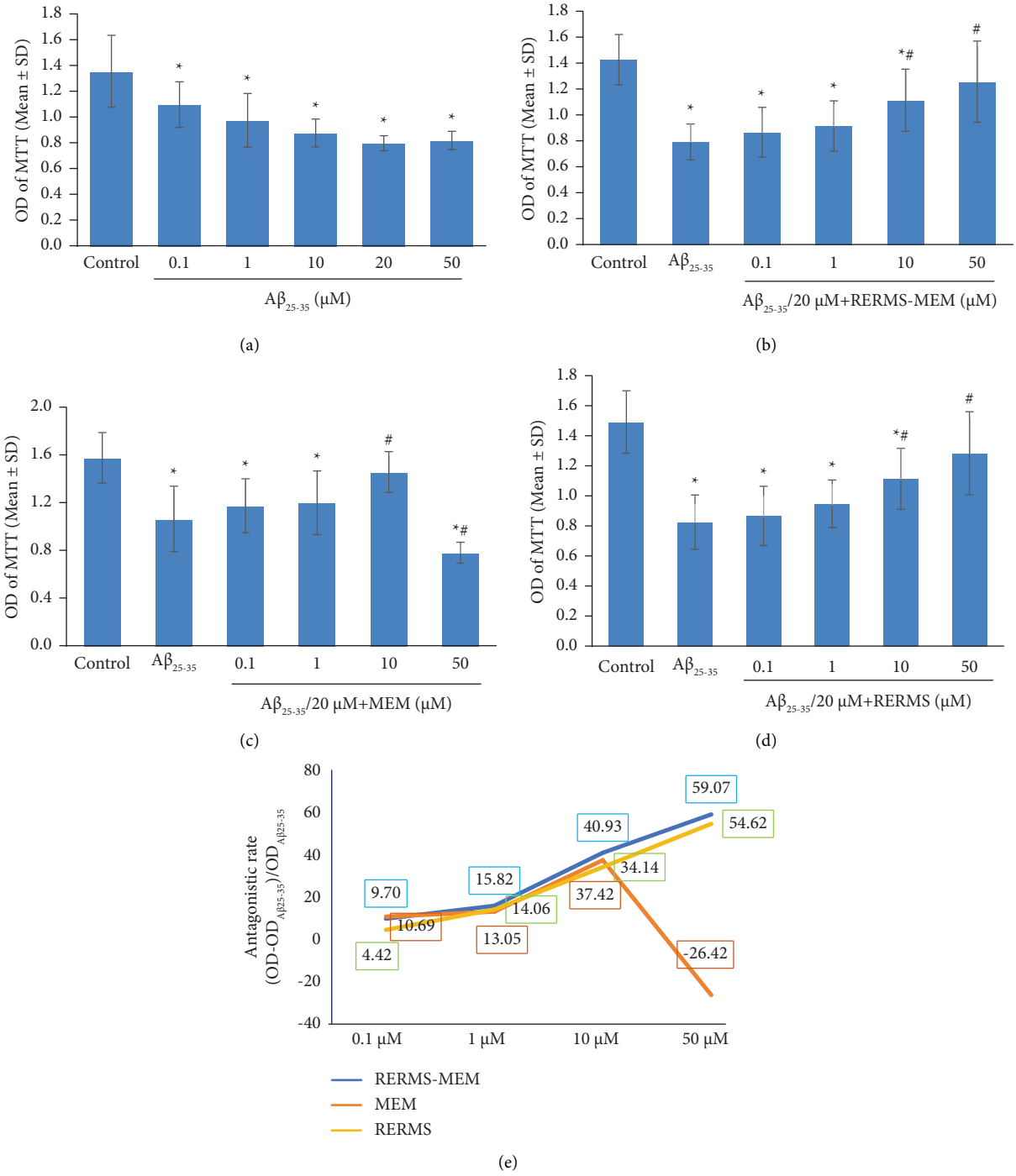

Figure 10: Antagonistic effect of RERMS-MEM, RERMS, and MEM for $A\beta_{25-35}$-induced neurotoxicity in SH-SY5Y cells: (a) toxic effect of $A\beta_{25-35}$ on SH-SY5Y cells; (b) antagonistic effect of RERMS-MEM for $A\beta_{25-35}$-induced neurotoxicity in SH-SY5Y cells; (c) antagonistic effect of MEM for $A\beta_{25-35}$-induced neurotoxicity in SH-SY5Y cells; (d) antagonistic effect of RERMS for $A\beta_{25-35}$-induced neurotoxicity in SH-SY5Y cells; (e) antagonistic rate of RERMS-MEM, RERMS, and MEM for $A\beta_{25-35}$-induced neurotoxicity in SH-SY5Y cells; $^{*}p < 0.05$ versus the control; $^{\#}p < 0.05$ versus $A\beta_{25-35}$. The values are shown as the mean ± SD.

5. Conclusion

In general, RERMS-MEM, as a potential NMDAR antagonist, enhanced the metabolic rate and promoted cellular growth, showing a neurotrophic effect in SH-SY5Y cells at a low dose. In addition, no cytotoxic effect was observed for RERMS-MEM at a high dose. Considering its promising utilization against AD, this modified drug is considered worthy of further development. In future studies, our efforts will be focused on further characterization of RERMS-MEM through a series of experiments in animal models of AD.

Abbreviations

AD: Alzheimer's disease
ADMET: Adequate absorption, distribution, metabolism, excretion, and tolerable toxicity
AβPP: Amyloid precursor protein
AβPP 17: AβPP 17-mer peptide
BBB: Blood brain barrier
CADD: Computer-aided drug design
CCK-8: Cell counting kit-8
DCC: N, N′-Dicyclohexylcarbodiimide
DMF: N, N-Dimethylformamide
DMSO: Dimethyl sulfoxide
HATU: 2-(7-Azabenzotriazol-1-yl)-N,N,N′,N′-tetramethyluronium hexafluorophosphate
HOBt: Hydroxybenzotriazole
HPLC: High-performance liquid chromatography
LDH: Lactate dehydrogenase
MEM: Memantine
MTT: Dimethylthiazol-2-yl-2,5-diphenyltetrazolium bromide
NMM: N-Methyl morpholine
NMDAR: N-Methyl-D-aspartate receptor
NMDAR2B: N-Methyl-D-aspartate receptor type 2B
RERMS: AβPP 5-mer peptide
RERMS-MEM: Arg-Glu-Arg-Met-Ser-(3,5)-dimethyladamantan-1-amine
Rg: Radius of gyration
RMSD: Root mean square deviation
RMSF: Root mean square fluctuation
SPR: Surface plasmon resonance
THF: Tetrahydrofuran
TLC: Thin-layer chromatography.

Data Availability

The data that support the findings of this study are included within the article and in supplementary materials.

Conflicts of Interest

The authors declare that they have no conflicts of interest.

Acknowledgments

This article was supported by the National Key R&D Program of China of the Ministry of Science and Technology of the People's Republic of China (grant no. 2018YFA0108503), the Capital Health Development Research Project of the Beijing Municipal Health Commission (grant no. 2020-2Z-1034), the National Natural Science Foundation of China (grant no.: 82001388), the National Key R&D Program of China (grant no. 2022YFC2403500), and the Capital Medical University Cultivation Fund (grant no. PYZ22044).

Supplementary Materials

Figure S1: ESI (+)-FT-ICR-MS of RERMS-MEM. Figure S2: ^{1}H NMR of RERMS-MEM. Figure S3: ^{13}C NMR of RERMS-MEM. Figure S4: HPLC of RERMS-MEM. Figure S5: ESI (+)-Q-TOF-MS of N-Boc-Arg (NO_2)-Glu (OBzl)-Arg (NO_2)-Met-Ser-(3,5)-dimethyladamantan-1-amine. Figure S6: ^{1}H NMR of N-Boc-Arg (NO_2)-Glu (OBzl)-Arg (NO_2)-Met-Ser-(3,5)-dimethyladamantan-1-amine. (*Supplementary Materials*)

References

[1] F. De and M. V. Lourenco, "Brain metabolic stress and neuroinflammation at the basis of cognitive impairment in Alzheimer's disease," *Frontiers in Aging Neuroscience*, vol. 7, p. 94, 2015.
[2] F. G. De Felice, "Alzheimer's disease and insulin resistance: translating basic science into clinical applications," *Journal of Clinical Investigation*, vol. 123, no. 2, pp. 531–539, 2013.
[3] A. Peruffo and B. Cozzi, "Bovine brain: an in vitro translational model in developmental neuroscience and neurodegenerative research," *Frontiers in pediatrics*, vol. 2, p. 74, 2014.
[4] H. Jahn, "Memory loss in Alzheimer's disease," *Dialogues in Clinical Neuroscience*, vol. 15, no. 4, pp. 445–454, 2013.
[5] K. Nakazawa, T. J. McHugh, M. A. Wilson, and S. Tonegawa, "NMDA receptors, place cells and hippocampal spatial memory," *Nature Reviews Neuroscience*, vol. 5, pp. 361–372, 2004.
[6] X. Song, M. Jensen, V. Jogini et al., "Mechanism of NMDA receptor channel block by MK-801 and memantine," *Nature*, vol. 556, no. 7702, pp. 515–519, 2018.
[7] I. G. Tikhonova, I. I. Baskin, V. A. Palyulin, N. S. Zefirov, and S. O. Bachurin, "Structural basis for understanding Structure−Activity relationships for the glutamate binding site of the NMDA receptor," *Journal of Medicinal Chemistry*, vol. 45, no. 18, pp. 3836–3843, 2002.
[8] D. Świetlik, J. Białowąs, A. Kusiak, and M. Krasny, "Virtual Therapy with the NMDA Antagonist Memantine in Hippocampal Models of Moderate to Severe Alzheimer's Disease, in Silico Trials," *Pharmaceuticals*, vol. 15, p. 546, 2022.
[9] S. Thakral, A. Yadav, V. Singh et al., "Alzheimer's disease: molecular aspects and treatment opportunities using herbal drugs," *Ageing Research Reviews*, vol. 88, Article ID 101960, 2023.
[10] S. M. Hoy, "Lecanemab: first approval," *Drugs*, vol. 83, no. 4, pp. 359–365, 2023.
[11] S. Kumari, K. Maddeboina, R. D. Bachu, S. H. S. Boddu, P. C. Trippier, and A. K. Tiwari, "Pivotal role of nitrogen heterocycles in Alzheimer's disease drug discovery," *Drug Discovery Today*, vol. 27, no. 10, Article ID 103322, 2022.
[12] T. Lengauer and M. Rarey, "Computational methods for biomolecular docking," *Current Opinion in Structural Biology*, vol. 6, no. 3, pp. 402–406, 1996.
[13] M. De Vivo, M. Masetti, G. Bottegoni, and A. Cavalli, "Role of molecular dynamics and related methods in drug discovery," *Journal of Medicinal Chemistry*, vol. 59, no. 9, pp. 4035–4061, 2016.
[14] S. A. Lipton, "Pathologically-activated therapeutics for neuroprotection: mechanism of NMDA receptor block by memantine and S-nitrosylation," *Current Drug Targets*, vol. 8, no. 5, pp. 621–632, 2007.
[15] S. A. Lipton, "Paradigm shift in neuroprotection by NMDA receptor blockade: memantine and beyond," *Nature Reviews Drug Discovery*, vol. 5, no. 2, pp. 160–170, 2006.
[16] M. Allgaier, "An update on drug treatment options of Alzheimer's disease," *Frontiers in Bioscience*, vol. 19, no. 8, p. 1345, 2014.

[17] L. S. Schneider, F. Mangialasche, N. Andreasen et al., "Clinical trials and late-stage drug development for Alzheimer's disease: an appraisal from 1984 to 2014," *Journal of Internal Medicine*, vol. 275, no. 3, pp. 251–283, 2014.

[18] D. Jantas, M. Pytel, J. W. Mozrzymas et al., "The attenuating effect of memantine on staurosporine-salsolinol- and doxorubicin-induced apoptosis in human neuroblastoma SH-SY5Y cells," *Neurochemistry International*, vol. 52, no. 4-5, pp. 864–877, 2008.

[19] W. Liu, Z. Xu, T. Yang, B. Xu, Y. Deng, and S. Feng, "Memantine, a low-affinity NMDA receptor antagonist, protects against methylmercury-induced cytotoxicity of rat primary cultured cortical neurons, involvement of Ca2+ dyshomeostasis antagonism, and indirect antioxidation effects," *Molecular Neurobiology*, vol. 54, no. 7, pp. 5034–5050, 2017.

[20] T. Kos and P. Popik, "A comparison of the predictive therapeutic and undesired side-effects of the NMDA receptor antagonist, memantine, in mice," *Behavioural Pharmacology*, vol. 16, no. 3, pp. 155–161, 2005.

[21] G. Marotta, F. Basagni, M. Rosini, and A. Minarini, "Memantine derivatives as multitarget agents in Alzheimer's disease," *Molecules*, vol. 25, no. 17, p. 4005, 2020.

[22] K. K. Spilovska, J. Korabecny, A. Horova et al., "Design, synthesis and in vitro testing of 7-methoxytacrine-amantadine analogues: a novel cholinesterase inhibitors for the treatment of Alzheimer's disease," *Medicinal Chemistry Research*, vol. 24, no. 6, pp. 2645–2655, 2015.

[23] K. Spilovska, J. Korabecny, J. Kral et al., "7-Methoxytacrine-Adamantylamine heterodimers as cholinesterase inhibitors in Alzheimer's disease treatment— synthesis, biological evaluation and molecular modeling studies," *Molecules*, vol. 18, no. 2, pp. 2397–2418, 2013.

[24] M. Kaniakova, E. Nepovimova, L. Kleteckova et al., "Combination of memantine and 6-chlorotacrine as novel multitarget compound against Alzheimer's disease," *Current Alzheimer Research*, vol. 16, no. 9, pp. 821–833, 2019.

[25] E. Simoni, S. Daniele, G. Bottegoni et al., "Combining galantamine and memantine in multitargeted, new chemical entities potentially useful in Alzheimer's disease," *Journal of Medicinal Chemistry*, vol. 55, no. 22, pp. 9708–9721, 2012.

[26] S. O. Bachurin, E. F. Shevtsova, G. F. Makhaeva et al., "Novel conjugates of aminoadamantanes with carbazole derivatives as potential multitarget agents for AD treatment," *Scientific Reports*, vol. 7, no. 1, Article ID 45627, 2017.

[27] M. Rosini, E. Simoni, R. Caporaso et al., "Merging memantine and ferulic acid to probe connections between NMDA receptors, oxidative stress and amyloid-β peptide in Alzheimer's disease," *European Journal of Medicinal Chemistry*, vol. 180, pp. 111–120, 2019.

[28] P. Sozio, L. S. Cerasa, S. Laserra et al., "Memantine-sulfur containing antioxidant conjugates as potential prodrugs to improve the treatment of Alzheimer's disease," *European Journal of Pharmaceutical Sciences*, vol. 49, no. 2, pp. 187–198, 2013.

[29] F. T. Zindo, Q. R. Barber, J. Joubert, J. J. Bergh, J. P. Petzer, and S. F. Malan, "Polycyclic propargylamine and acetylene derivatives as multifunctional neuroprotective agents," *European Journal of Medicinal Chemistry*, vol. 80, pp. 122–134, 2014.

[30] T. Kumamoto, M. Nakajima, R. Uga et al., "Design, synthesis, and evaluation of polyamine-memantine hybrids as NMDA channel blockers," *Bioorganic & Medicinal Chemistry*, vol. 26, no. 3, pp. 603–608, 2018.

[31] O. Karoutzou, S. H. Kwak, S. D. Lee et al., "Towards a novel class of multitarget-directed ligands: dual P2X7–NMDA receptor antagonists," *Molecules*, vol. 23, no. 1, p. 230, 2018.

[32] M. Duque, P. Camps, E. Torres et al., "New oxapolycyclic cage amines with NMDA receptor antagonist and trypanocidal activities," *Bioorganic & Medicinal Chemistry*, vol. 18, no. 1, pp. 46–57, 2010.

[33] B. Feng, H. Peng, S. J. Lu, W. Rong, and Y. F. Du, "Effects of APP 5-mer peptide analogue P165 on the synaptic proteins and insulin signal transduction proteins," *International Journal of Clinical and Experimental Medicine*, vol. 7, p. 549, 2014.

[34] P. Wang, S. Jiang, Y. Cui et al., "The n-terminal 5-MER peptide analogue P165 of amyloid precursor protein exerts protective effects on SH-SY5Y cells and rat hippocampus neuronal synapses," *Neuroscience*, vol. 173, pp. 169–178, 2011.

[35] J. Yao, L. Ma, R. Wang, S. Sheng, Z. Ji, and J. Zhang, "Neurotrophic effects of amyloid precursor protein peptide 165 in vitro," *Brain Research Bulletin*, vol. 120, pp. 58–62, 2016.

[36] R. Mileusnic, C. L. Lancashire, and S. Rose, "The peptide sequence Arg-Glu-Arg, present in the amyloid precursor protein, protects against memory loss caused by Abeta and acts as a cognitive enhancer," *European Journal of Neuroscience*, vol. 19, no. 7, pp. 1933–1938, 2004.

[37] J. Wu, H. Zhu, M. Zhao et al., "IQCA-TASS: a nano-scaled P-selectin inhibitor capable of targeting thrombus and releasing IQCA/TARGD(S)S in vivo," *Journal of Materials Chemistry B*, vol. 5, pp. 917–927, 2017.

[38] X. Hu, M. Zhao, Y. Wang et al., "Tetrahydro-β-carboline-3-carboxyl-thymopentin: a nano-conjugate for releasing pharmacophores to treat tumor and complications," *Journal of Materials Chemistry B*, vol. 4, no. 8, pp. 1384–1397, 2016.

[39] E. C. Suh, Y. J. Jung, Y. A. Kim, E. M. Park, S. J. Lee, and K. E. Lee, "Knockout of Toll-like receptor 2 attenuates Aβ25–35-induced neurotoxicity in organotypic hippocampal slice cultures," *Neurochemistry International*, vol. 63, no. 8, pp. 818–825, 2013.

[40] J. Jia, X. Zhang, G. Xu, X. Zeng, and L. Li, "Thioredoxin-1 inhibits amyloid-β25–35-induced activation of NLRP1/caspase-1/GSDMD pyroptotic pathway in PC12 cells," *Molecular Biology Reports*, vol. 49, no. 5, pp. 3445–3452, 2022.

[41] X. Pei, F. Hu, F. Luo et al., "The neuroprotective effects of alpha-lipoic acid on an experimental model of Alzheimer's disease in PC12 cells," *Journal of Applied Toxicology*, vol. 42, no. 2, pp. 285–294, 2022.

[42] J. Folch, O. Busquets, M. Ettcheto et al., "Memantine for the treatment of dementia: a review on its current and future applications," *Journal of Alzheimer's Disease*, vol. 62, no. 3, pp. 1223–1240, 2018.

[43] E. Karakas and H. Furukawa, "Crystal structure of a heterotetrameric NMDA receptor ion channel," *Science*, vol. 344, no. 6187, pp. 992–997, 2014.

[44] C. H. Lee, W. Lü, J. C. Michel et al., "NMDA receptor structures reveal subunit arrangement and pore architecture," *Nature*, vol. 511, no. 7508, pp. 191–197, 2014.

[45] G. Small and B. Dubois, "A review of compliance to treatment in Alzheimer's disease: potential benefits of a transdermal patch," *Current Medical Research and Opinion*, vol. 23, no. 11, pp. 2705–2713, 2007.